PHYSICAL REVIEW E **00**, 002400 (2016)

Geometry optimization of branchings in vascular networks

Jamel Khamassi,[1,2,3,*] Claas Bierwisch,[2] and Peter Pelz[3]
[1] *University of Freiburg, Institute of Physics, Hermann-Herder-Str. 3a, 79104 Freiburg, Germany*
[2] *Fraunhofer IWM, Wöhlerstr. 11, 79108 Freiburg, Germany*
[3] *Technische Universität Darmstadt, Chair of Fluid Systems, Magdalenenstr. 4, 64289 Darmstadt, Germany*
(Received 17 December 2015; published xxxxxx)

Progress has been made in developing manufacturing technologies which enable the fabrication of artificial vascular networks for tissue cultivation. However, those networks are rudimentary designed with respect to their geometry. This restricts long-term biological functionality of vascular cells which depends on geometry-related fluid mechanical stimuli and the avoidance of vessel occlusion. In the present work, a bioinspired geometry optimization for branchings in artificial vascular networks has been conducted. The analysis could be simplified by exploiting self-similarity properties of the system. Design rules in the form of two geometrical parameters, i.e., the branching angle and the radius ratio of the daughter branches, are derived using the wall shear stress as command variable. The numerical values of these parameters are within the range of experimental observations. Those design rules are not only beneficial for tissue engineering applications. Moreover, they can be used as indicators for diagnoses of vascular diseases or for the layout of vascular grafts.

DOI: 10.1103/PhysRevE.00.002400

I. INTRODUCTION

An inadequate hemodynamic wall shear stress (WSS) has been identified as the key factor for atherosclerosis initiation in the past decades [1]. The homogeneity of the WSS distribution is particularly disturbed in curvatures and bifurcations. The blood flow patterns which accompany strongly inhomogeneous stress distributions were discovered to cause atherosclerosis [2]. The primary goal of the present study is to correlate geometrical properties of vascular bifurcations with the associated WSS distributions. Presuming that homogeneous hemodynamic stimulations exist within healthy natural vascular structures, numerically optimized geometries with regard to the shear stress distribution should resemble physiological geometries of vascular branchings. In terms of tissue engineering and the manufacturing of endothelialized artificial vascular networks, design rules can be derived from such optimized geometries in order to ensure physiological stimulation and to prevent clogging.

A. Role of endothelium

In natural vascular systems endothelium plays an important role in the supply of the surrounding tissue. The endothelium is the inner cell layer of every blood vessel and controls the exchange of oxygen, nutrients, and metabolic waste products between the blood and the tissue. It also supports the wound healing by the formation of clots [3]. In addition, endothelium participates in angiogenesis which is the natural mechanism of blood flow regulation by sprouting of new vessels from existing ones. The angiogenesis is stimulated by vascular endothelial growth factor (VEGF) proteins which are produced by cells if their oxygen supply decreases [4]. Because of the limited oxygen diffusion range of 20 to 100 μm in tissue the vascular network is continuously reorganizing itself in order to supply all surrounding tissue cells properly [5]. The prosperity of endothelial cells depends on mechanical stimulation caused by flow induced WSS. Essential biochemical reactions and gene expressions of the endothelium occur in response to a WSS of about 1 to 5 Pa [6,7]. In healthy vascular vessels the shear stress perceived by the endothelium is considered to lie within this range. Low WSS ($<$1 Pa) coincides with prolonged flow residence times which can cause plaque deposition leading to flow restrictions and diseases such as atherosclerosis [2]. The endothelial response to WSS larger than 1.5 Pa induces a gene expression which protects against mechanisms leading into atherosclerosis [2]. It also hinders platelet adhesion by secretion of prostacyclin and nitric oxide [8]. Thus the lowest occurring WSS in a blood vessel should exceed 1 Pa or preferably even 1.5 Pa. Figure 1 shows a simplified vascular branching where the contour lines denote the shear stress. While the WSS along the right branch is rather homogeneous and above 1.5 Pa, the left branch shows a distinct region of low WSS. The latter region bears a risk to become pathological which can be explained by the above mentioned shear stress requirements. In summary, the occurrence of atherosclerosis can be considered as a consequence of an inappropriate vascular geometry leading to regions of low WSS.

B. Optimal vascular networks

An early approach to derive geometric properties of a vascular network from fundamental principles is based on the minimization of the sum of the energy required for pumping blood through the network and the energy required for the metabolic supply of the blood volume. This optimization yields Murray's law, a formula for the relation between the radius R_0 of the parent vessel and the radii $R_{1,2}$ of the daughter vessels at branching points [9]:

$$R_0^3 = R_1^3 + R_2^3. \tag{1}$$

Murray's law was successfully applied to describe the layout of natural vascular systems with several branching levels [10]. Kassab *et al.* showed that Murray's law in combination with a constant pressure gradient model yields a constant WSS

*jamel.khamassi@iwm.fraunhofer.de

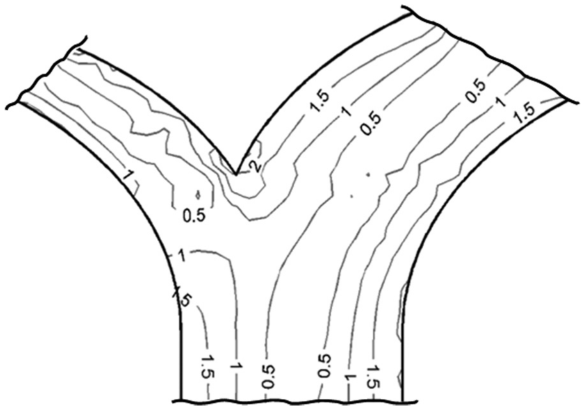

FIG. 1. Shear stress distribution in Pa in a schematic vascular bifurcation.

throughout the system [11]. Kamiya *et al.* developed a more detailed formulation for an optimal vascular tree structure than Murray by taking into account the hydrodynamic resistance of the system as well as pressure boundary conditions at chosen inlet and outlet positions [12]. In combination with a volume minimization routine, optimal positions of the branching points were obtained. Several recent studies applied these optimization approaches to large vascular structures. In Ref. [13] three-dimensional vascular trees were simulated. In Ref. [14] a routine was developed to build vascular structures within concave volumes such as the free wall of the left ventricle of the heart. The growth of blood vessels caused by the demand of oxygen is considered in Ref. [15]. This study contains an iterative scheme for vascular structure development based on a user defined demand map. All of the mentioned studies have in common that they assume a network consisting of straight tubes between the branching points. The actual geometries of vascular branchings are neglected and, hence, no details on the flow field and the related stimulation of the endothelium due to the WSS can be provided. As pathological flow conditions at bifurcations (e.g., low WSS and long residence times) can dramatically reduce the functionality of a vascular system, it is sensible to ask whether optimal branching geometries with respect to endothelium stimulation and occlusion avoidance exist. One objective of the current study is to answer this question.

C. Experimentally observed branching geometries

Kassab *et al.* analyzed the morphometry of the coronary arterial and venous trees of four pig hearts [16,17]. The purpose of this study is to assign vessel orders based on the diameter. The authors argue that the diameter distribution is important for the hemodynamic properties within the vascular structure. The idea of this work was to characterize the full vascular tree of a low number of structures in great detail rather than many structures marginally. Those morphometric measurements are performed with a silicone elastomer casting method. A database of diameter and length information of the full vascular tree is determined. Within their study they provide a connectivity matrix which resembles the vascular tree and categorize each vessel with an order number. Thus, for every bifurcation, the vessel order of the parent branch and its daughter branches is characterized by their spatial dimensions. The authors found that 98% of the arterial branchings are bifurcations and only 2% are trifurcations. The number of vessels assigned to each vessel order is summarized in the obtained vascular tree. It should be noted that for the flow pattern within a bifurcation the branching angle is a key parameter besides the vessel diameters.

Cassot *et al.* created a database in which nearly 10 000 bifurcations of cortical vascular trees were analyzed [18]. Their data provides a statistical basis for two quantities of interest of the two daughter vessels of a bifurcation, i.e., the ratio of their cross-sectional areas and the branching angle between them. Concerning Eq. (1) the study confirms an exponent of approximately 3 for larger vessels while an exponent tending towards 4 is found for smaller vessels. Based on these results the authors argue *"that such a law (and perhaps the optimal design principle that underpins it) is ultimately unable to account for the true complexity found within the architecture of microvascular branching"*. Taking into account all bifurcations, the area ratio was found to be 0.686 ± 0.213 and the branching angle $103.8^\circ \pm 27.4^\circ$. These values will be compared with the results obtained in the present study.

D. Tissue engineering and artificial vascular vessels

Currently, the lack of donor organs limits the potential of transplantation medicine. *In vitro* grown tissue could be a solution for this shortage. According to Ref. [19], the key challenge in tissue engineering is the existence of perfusable vascular networks in order to supply the cultivated cells on a sustained basis with oxygen and nutrients. Cells rapidly develop necrotic cores if their supply is insufficient. Thus the development of artificial vascular systems with physiological functionality would be a breakthrough for *in vitro* cell cultivation. Recent publications demonstrate the possibility of angiogenesis in artificial vascular systems [20,21]. Endothelium layers could be settled in artificial structures built of biocompatible materials. These results are milestones in the fabrication of transportation systems for nutrients and metabolic by-products. However, the long-term functionality of artificial vascular systems remains unproven. The design rules for vascular branchings obtained in the current study could be an important building block for such artificial supply networks.

The paper is organized as follows. The next section illustrates the geometry of the branching model, the computational fluid dynamics methods which are applied, and the analyses which are conducted. The obtained results are then demonstrated and discussed in comparison to experimental findings. Finally, concluding remarks and an outlook are given.

II. METHODS

A. Model geometry

The present study takes into account a single bifurcation under physiological flow conditions. Figure 2 provides a brief schematic overview of all parameters of the observed system. These are the fluid's velocity $\vec{u}$, density ρ, and viscosity η, the radius of the parent vessel R_0, the radii of the daughter vessels $R_{1,2}$, and the branching angle α.

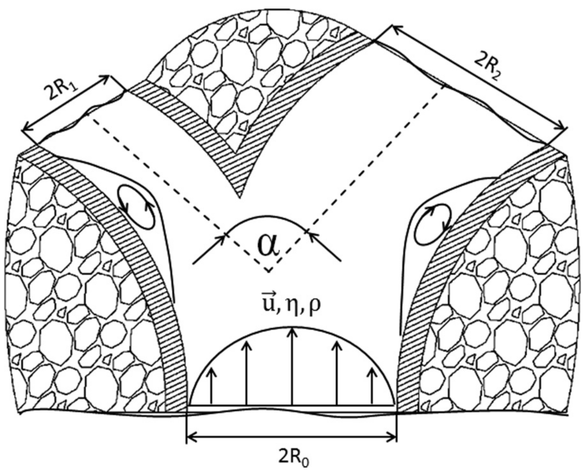

FIG. 2. Parameters and model description.

Blood vessels are self-similar at different length scales [22]. Thus, within a certain range of vessel diameters, vascular branchings of different size show comparable flow profiles. Similarities in flow patterns are, on one hand, limited for small vessels by the ratio between the lumen diameter and the diameter of the red blood cells and, on the other hand, for big vessels by high Reynolds numbers due to the laminar-turbulent transition. Those limiting conditions are found in capillaries and the aorta, respectively. For the course of this study we reduce the geometry of each bifurcation into its asymmetry ratio and its branching angle α. The asymmetry ratio is defined as

$$R^{+} = \frac{R_1}{R_2}, \tag{2}$$

where R_1 is the radius of the smaller and R_2 of the larger daughter vessel (compare Fig. 2). According to the findings of Cassot *et al.* [18] there exists no single exponent of 3 for the relation of the branch radii, i.e., Eq. (1). The exponent is rather found to depend on the vessel size and the type of bifurcation. Even though the exponent might not be exactly 3 for every observed bifurcation, Murray's law is assumed to provide a reasonable average. This assumption is based on the findings of a series of studies which confirm this exponent [23–25]. Thus, for the models analyzed here, an exponent of 3 has been used in Eq. (1). The radii of the daughter branches for asymmetry ratios R^+ in the range from 0.25 to 1.0 are shown in Fig. 3. Note that the radius of the smaller branch increases stronger with R^+ than the radius of the larger branch decreases. At a ratio $R^+ = 1.0$ both daughter branch radii are equal by definition. Figure 4 shows the fluid domain used for the numerical simulations of the flow in the bifurcation. Based on the method proposed in Ref. [18], the branching angle is defined as follows: the daughter branches are considered to lead into straight extensions indicated by the dashed lines in Fig. 4. Within each daughter branch two circles touching the vessel walls are placed. The center of one of these circles lies within the simulated fluid domain and the center of the other circle out of the domain. The vectors connecting the center points of the circles in both branches span the branching angle α.

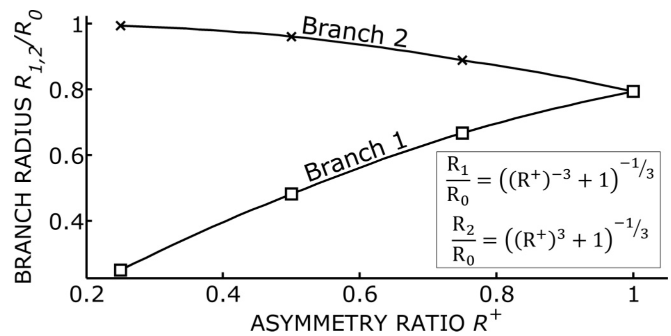

FIG. 3. Branch radii as a function of the asymmetry ratio.

B. Computational fluid dynamics (CFD) approach

A numerical model is built in two dimensions which takes into account the blood flow and the elastic response of the vessel wall. Deformations of the fluid domain are calculated with an arbitrary Lagrangian Eulerian (ALE) scheme [26].

This scheme treats the fluid domain by conserving mass and momentum in the way presented in Eqs. (3) and (4),

$$\nabla \cdot \vec{u} = 0, \tag{3}$$

$$\rho\left(\frac{\partial \vec{u}}{\partial t} + \vec{u} \cdot \nabla \vec{u}\right) = -\nabla p + \eta \Delta \vec{u}. \tag{4}$$

The symbols $\vec{u}$, t, ρ, p, and η are the velocity, time, density, pressure, and viscosity, respectively. The equations model an incompressible fluid which is considered in the present work. On the right-hand side of the Navier-Stokes equation (4) the divergence of the stress tensor is expressed as the sum of the pressure gradient and the Laplacian of the velocity multiplied by the viscosity. The Laplacian of the velocity is related to the divergence of the strain rate tensor $\mathbf{D}$ via $\Delta \vec{u} = 2\nabla \cdot \mathbf{D}$.

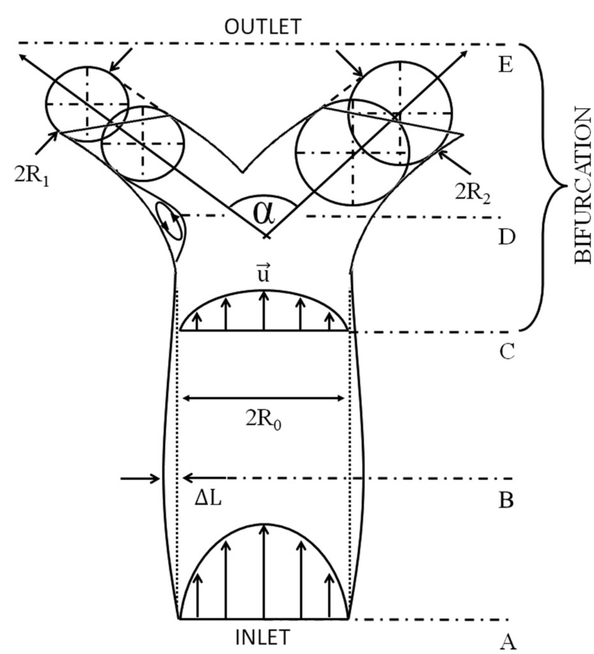

FIG. 4. Sketch of the fluid domain including the definition of the branching angle. The symbols are defined in the text.

The momentum equation for the structural problem of the solid domain (vessel walls),

$$\rho \frac{\partial^2 \vec{x}}{\partial t^2} = \nabla \cdot \boldsymbol{\sigma}, \tag{5}$$

evolves the displacement $\vec{x}$ according to the Cauchy stress tensor $\boldsymbol{\sigma}$. We distinguish between a stiff and an elastic approach. For stiff walls, the displacement is zero and the complete problem reduces to the fluid dynamics equations (3) and (4). For elastic walls, linear elasticity is applied by Hooke's law, $\boldsymbol{\sigma} = C\,\boldsymbol{\epsilon}$, where C denotes the elasticity tensor and $\boldsymbol{\epsilon}$ is the linearized strain tensor,

$$\boldsymbol{\epsilon} = \frac{1}{2}(\nabla\vec{x} + (\nabla\vec{x})^T). \tag{6}$$

Hooke's law can be simplified for isotropic material behavior as follows:

$$\boldsymbol{\sigma} = \frac{Y}{1+\nu}\boldsymbol{\epsilon} + \frac{Y\nu}{(1+\nu)(1-2\nu)}(\nabla\cdot\vec{x})\mathbf{I}, \tag{7}$$

where Y, ν, and $\mathbf{I}$ denote Young's modulus, Poisson's ratio, and the unit tensor, respectively. Young's modulus is set to 1.2 MPa and Poisson's ratio to 0.3. A no slip condition is applied at the interface of the fluid and solid domain. The coupling between both domains is realized by the equivalence of mechanical stresses and displacements.

The Navier-Stokes equations are solved for a single phase fluid with complex rheological properties in order to model blood. The interactions of red blood cells lead to a shear thinning behavior of the viscosity with increasing shear rate $\dot{\gamma}$ [27,28], which is applied in the present model in the form of the Carreau-Yasuda formulation [29]:

$$\eta(\dot{\gamma}) = \eta_\infty + (\eta_0 - \eta_\infty)[1 + (\lambda\dot{\gamma})^a]^{\frac{n-1}{a}}, \tag{8}$$

with the parameters $\eta_0 = 0.16$ Pa s, $\eta_\infty = 0.0035$ Pa s, $\lambda = 8.2$ s, $a = 0.64$, and $n = 0.2128$ determined experimentally [30]. The blood density is set to $\rho = 1000$ kg/m^3. At the vessel walls a no slip boundary condition is applied. The flow resistance depends on the actual bifurcation geometry. The resistances of different bifurcations will be compared by applying a pressure boundary condition and leaving the mass flux variable.

The parent vessel has a radius of $R_0 = 500$ μm which represents vessels ranging from arterioles to small arteries. A physiological, time dependent pressure for small arterial vessels is applied at the inlet of the fluid domain, i.e., position A in Fig. 4. The outlet condition is implemented as proposed in Ref. [31]. This approach consists of a solution for the outlet area, pressure, and volume flux, which avoids nonphysiological wave reflections. The outlet boundary condition is solved on a one-dimensional domain extending from each daughter branch. Therefore, the outlet is marked at position E in Fig. 4 in a reasonable distance from the two-dimensional simulation domain.

The Reynolds number Re of the studied system is defined as

$$\mathrm{Re} = \frac{2R_0\bar{u}\rho}{\eta_\infty}, \tag{9}$$

with the time averaged characteristic velocity $\bar{u}$ evaluated at the center of the vessel at the bifurcation entrance, i.e., at position C in Fig. 4, where the radius of the parent vessel starts to increase. The chosen model parameters and boundary conditions yield a Reynolds number of around 60 which is in agreement with the physiological observations of small arteries [32]. All numerical simulations within the present study were conducted using the finite element method solver Elmer. Further model and implementation details can be found in Ref. [33].

C. Wall shear stress analysis

We consider the WSS as the key parameter for the optimization of vascular branchings due to its physiological relevance for endothelium stimulation. Figure 1 shows the shear stress distribution in an asymmetric bifurcation. In this case, the WSS lies largely in the range between 1.5 and 2 Pa. At the corner of the bifurcation the WSS is somewhat elevated (>2 Pa), but still within the healthy range [6,7]. However, at the position of greatest curvature of the smaller branch, the WSS drops below 1 Pa which is a pathological situation. A low WSS value (i.e., <1 Pa) which often occurs in regions of stasis or stall is related to an increased plaque formation [34]. The WSS minimum occurring at the smaller branch curvature is identified as the major optimization parameter within this study. Its dependence on the bifurcation geometry is analyzed. The approximate location of lowest WSS is indicated schematically for geometries with varied asymmetry ratios R^+ and branching angles α in Fig. 5 by the arrows. Note that the location is dependent on the combination of those two geometry parameters.

A characteristic point in time t_0 is chosen for the WSS comparison between different geometries. t_0 is the time when the overall shear stress in the system is maximal. This may occur at slightly different absolute times depending on the actual geometry. Figure 4 illustrates the spatial positions where the analysis takes place at t_0. Position C denotes the bifurcation inlet where the parent branch flux is discussed. Since the vessel widening and contraction during a flow pulse influence the flux, the maximum vessel wall displacement ΔL is evaluated.

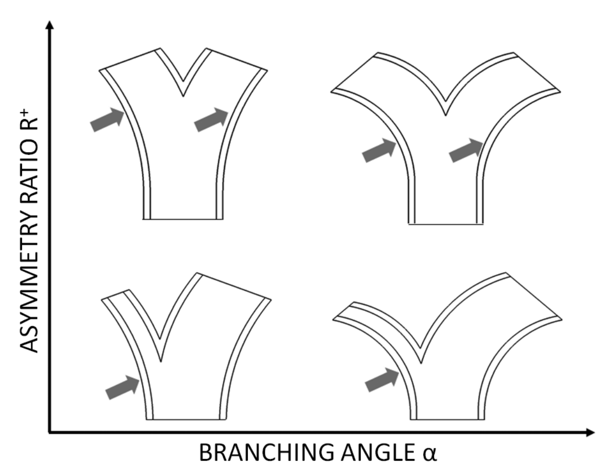

FIG. 5. Locations of minimum WSS for different bifurcation geometries.

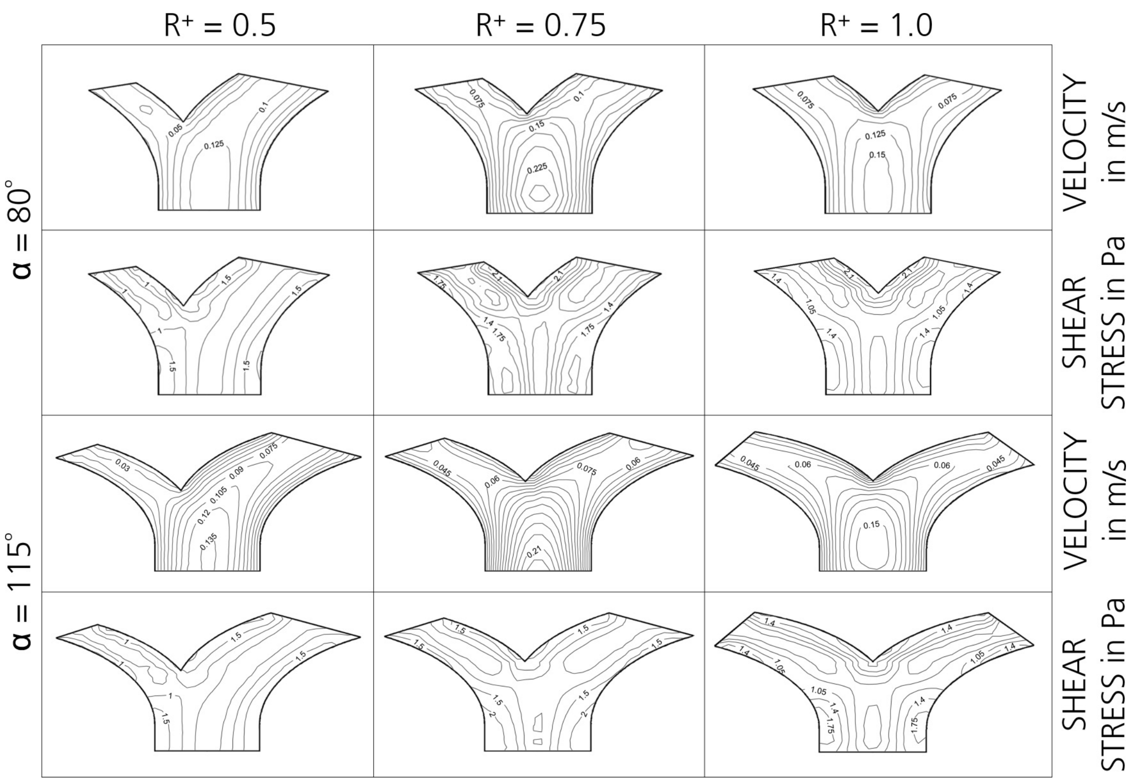

FIG. 6. Bifurcations with velocity and shear stress contour lines for different asymmetry ratios R^+ and branching angles α.

The maximum displacement occurs around position B. Around position D the minimal WSS occurs as indicated by the arrows in Fig. 5. The aim of this study is the identification of combinations of R^+ and α yielding a WSS distribution which lies completely in the range of nonpathological values. In order to do so, the minimal WSS is observed for different geometries under comparable flow conditions. The bifurcation geometry which yields the largest minimal WSS in comparison with the other geometries is considered to be optimal with respect to the avoidance of pathological flow conditions.

III. RESULTS

A. Wall shear stress

Figure 6 shows how the distributions of the velocity magnitude and the WSS are affected by the bifurcation geometry. Figure 5 highlights the pathological locations where the minimal WSS according to the analysis described in Sec. II C occurs. All bifurcation geometries which are studied are depicted as circles in Fig. 7 as a function of the asymmetry ratio R^+ and branching angle α. A Kriging metamodel [35] is utilized to approximate the WSS as a continuous function of the two geometry parameters. The present approach combines a local Kriging predictor with a global polynomial least square fit. The contour lines in Fig. 7 represent combinations of R^+ and α which yield equal minimal WSS values. The result of the metamodel appears to be roughly symmetric with respect to the observed range of branching angles α with a line of symmetry at about 90°. However, with respect to the range of asymmetry ratios R^+ the WSS result is noticeably divided into two subdomains. Within asymmetry ratios below $R^+ = 0.5$ the WSS increases with increasing R^+ but hardly any dependency on the branching angle is observed. Above $R^+ = 0.5$ a distinct WSS maximum can be observed for $R^+ = 0.769$ and $\alpha = 90.7°$. The metamodel predicts a value of 1.78 Pa for the WSS maximum. Since the maximum is obtained by a Kriging approach, its value is verified by an additional sample point which has not been used previously to calibrate the metamodel. The verification simulation yields 1.65 Pa which confirms the optimum with reasonable precision. It can be summarized that an optimal bifurcation geometry is identified with respect to the WSS analysis.

B. Mass flux

Although the optimal branching geometry has been identified, the reason for its shape is not yet clear. Therefore, the mass fluxes are studied in detail for the different branching

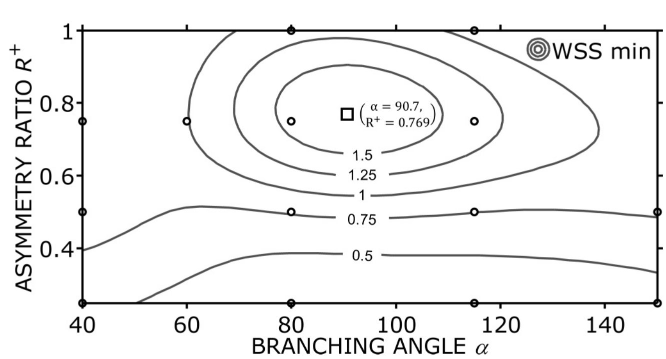

FIG. 7. Lowest WSS in Pa at t_0 (see text) as a function of the bifurcation geometry. Branching angle is expressed in degrees.

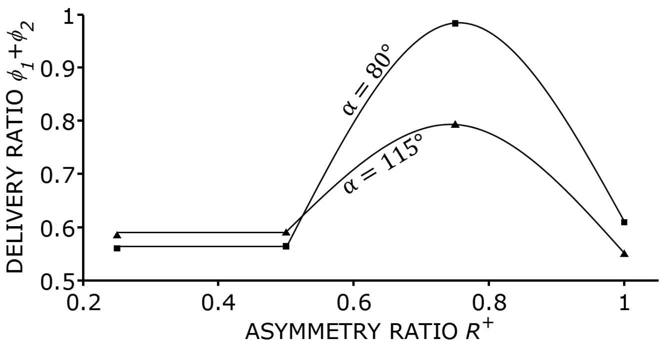

FIG. 8. Combined delivery ratios through the daughter branches for different bifurcation geometries.

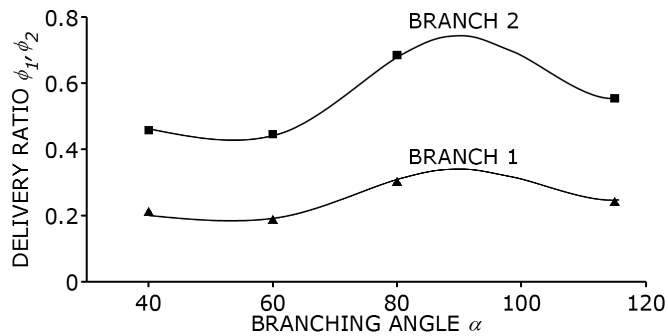

FIG. 9. Delivery ratios through the daughter branches as functions of the branching angle. The asymmetry ratio is constant at $R^+ = 0.75$.

angles and asymmetry ratios. We introduce the delivery ratio ϕ_i as a quotient of the actual flux through the daughter branch Q_i and a reference flux through the parent branch Q_0,

$$\phi_i = \frac{Q_i}{Q_0}. \tag{10}$$

The reference flux Q_0 is taken at time t_0 for the bifurcation with the properties $R^+ = 0.75$ and $\alpha = 80°$. Figure 8 shows the total delivery $\phi_1 + \phi_2$ through the daughter branches. Below $R^+ = 0.5$ the total delivery shows no pronounced dependency on R^+. However, around $R^+ = 0.75$ a maximal total delivery ratio is observed for both displayed branching angles of 80° and 115°. Thus the perfusing flux through the bifurcation is significantly higher compared to other asymmetry ratios. In addition, the flux through the bifurcation with $\alpha = 80°$ is significantly higher than for the case of 115°. The mass flux correlates directly with the WSS findings for both geometry properties. The resulting WSS depicted in Fig. 7 is a consequence of the variable perfusion. Of course, the flux itself is a function of the local flow resistance for a given bifurcation geometry.

In the following, both delivery ratios ϕ_1 and ϕ_2 are studied separately for the tested branching angles and asymmetry ratios. In each section, the flux through the daughter branches, the vessel wall displacement, and the perfusing flux without influence of the wall displacement are analyzed.

1. Branching angle

Figure 9 shows the delivery ratios of both daughter branches for the range of different branching angles. Below a branching angle of about 60° the flux is rather independent of the branching angle. For larger angles the flux increases. After reaching its maximum at around 90° the flux decreases again. A similar behavior is observed for the WSS in Fig. 7.

Figure 10 shows the vessel wall displacement within the parent branch for the observed range of branching angles. The displacement is monotonically increasing with the branching angle. For branching angles above 80° the displacement appears to saturate.

Figure 11 displays the results of an analysis similar to Fig. 9 but for a bifurcation with a rigid vessel wall and, thus, $\Delta L = 0$. Both delivery ratios are monotonically decreasing with the branching angle. The highest overall flux in a rigid bifurcation can be achieved for small branching angles, i.e., <60°. A rather weak dependency of the delivery ratio on the branching angle is observed in this range. A comparison of Fig. 9 and Fig. 11 with the WSS results in Fig. 7 hints that the optimal WSS at around 90° is related to the elasticity of the vessel wall.

2. Asymmetry ratio

Figure 12 shows the perfusion through both daughter branches for the range of studied asymmetry ratios. The WSS for a branch angle of 40° is below 1 Pa according to Fig. 7. In the case of $\alpha = 40°$ the flux through branch 1 increases while it decreases through branch 2 with increasing asymmetry ratio. This behavior resembles the branch radii variation as shown in Fig. 3. For a branching angle of 115° a different dependency on the asymmetry ratio is found. In this case, the flux through branch 2 has no pronounced dependency on R^+ for $R^+ \leqslant 0.75$, while the flux through branch 1 increases with R^+ comparable to the case of $\alpha = 40°$. As shown in Fig. 8, the sum $\phi_1 + \phi_2$ is constant for $R^+ \leqslant 0.5$, while it has a distinct maximum at $R^+ \approx 0.75$ due to the high flux through branch 1. For a branching angle of 80° the maximum flux through both of the daughter branches is obtained for $R^+ \approx 0.75$. The combination $\alpha = 80°$ and $R^+ = 0.75$ yields the maximum flux sum $\phi_1 + \phi_2$ (see also Fig. 8) as well as the highest WSS of all tested geometries (see Fig. 7). For all branching angles, the flux through branch 2 decreases with the asymmetry ratio for $R^+ > 0.75$. For symmetric bifurcations, i.e., $R^+ = 1$, the delivery ratios do not depend on the branching

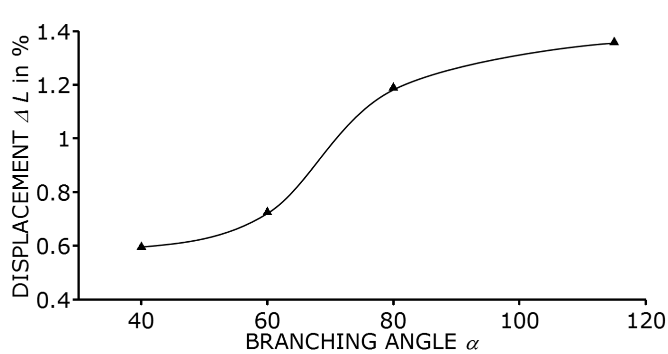

FIG. 10. Displacement of the parent branch as function of the branching angle. The asymmetry ratio is constant at $R^+ = 0.75$.

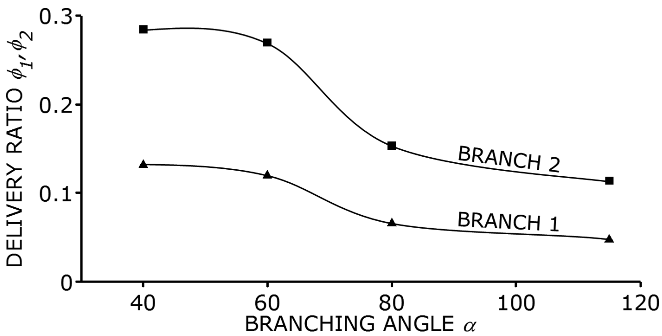

FIG. 11. Delivery ratios through the daughter branches without widening of the parent branch. The abscissa denotes the branching angle. The asymmetry ratio is constant at $R^+ = 0.75$.

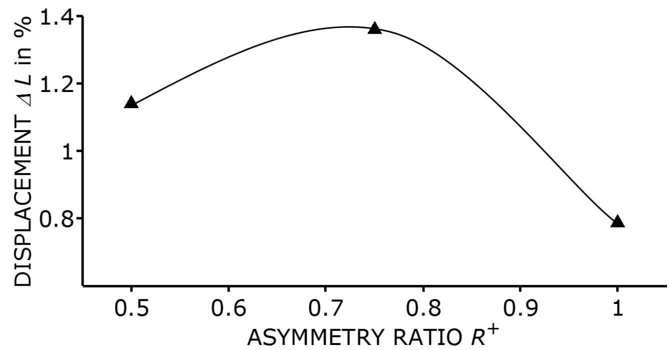

FIG. 13. Displacement of the parent branch as function of the asymmetry ratio. The branching angle is constant at $\alpha = 115^\circ$.

angle. Furthermore, the sum $\phi_1 + \phi_2$ is similar for $R^+ \leqslant 0.5$ and $R^+ = 1$ (see Fig. 8).

Figure 13 depicts the displacement of a bifurcation with a branching angle of 115° for the studied range of asymmetry ratios. The displacement is maximal for $R^+ \approx 0.75$ which also yields the largest flux sum (see Fig. 8). An asymmetry ratio larger than 0.75 leads to a decreasing displacement of the parent branch. The overall lowest displacement is found for a symmetric bifurcation.

In Fig. 14 the fluxes through the daughter branches are shown for a rigid vessel wall, i.e., $\Delta L = 0$. The highest flux sum is found for symmetric bifurcation, i.e., $R^+ = 1.0$. The asymmetry ratio of about 0.75 yields the lowest mass flux sum in this case, while it yielded the highest flux sum in the case of elastic vessel walls (see Fig. 8). Thus the maximization of the flux with respect to the branching angle and asymmetry ratio is apparently dependent on the vessel elasticity.

IV. DISCUSSION

Figures 11 and 14 show that the bifurcation geometry which yields the optimal WSS for a rigid vessel differs from the geometry obtained for an elastic vessel (see Fig. 7). For a rigid vessel, the optimum is a symmetrical geometry with the smallest possible branching angle. Thus the elasticity has a major influence on the optimal design. In the course of this discussion it will be pointed out that this influence of elasticity also applies for natural vascular branchings. Due to the elastic deformation and the following restoring force caused by the vessel wall, the fluid pressure at the bifurcation inlet, i.e., position C in Fig. 4, is higher in comparison to a rigid wall. Therefore, the pressure drop throughout the bifurcation is higher as well. As a consequence, the perfusion through the bifurcation is increased. The counteracting mechanism is the flow resistance within individual branches which reduces the perfusion.

In the following, the influences of branching angle and asymmetry ratio are discussed in detail.

A. Branching angle

The surprising observation is that a distinct optimum of WSS (or total flux) exists with respect to the branching angle. A bifurcation forms an additional resistance for the fluid flowing through the straight parent branch. Increasing the branching angle also increases the resistance experienced by the blood flow. Due to the curved branches the flow momentum is redirected and viscous effects increase the resistance throughout the daughter branches. The fluid is impounded in front of the bifurcation, which leads to a local pressure rise due to the deceleration. For an elastic vessel, the wall displacement ΔL increases with the pressure rise until it saturates for high branching angles (see Fig. 10). Since the elastic wall eventually restores its initial shape and, thereby, accelerates the fluid, the increase in flux for angles below 90° can be explained by the pressure drop over the bifurcation. However, the mass flux in both daughter branches decreases again for branching angles

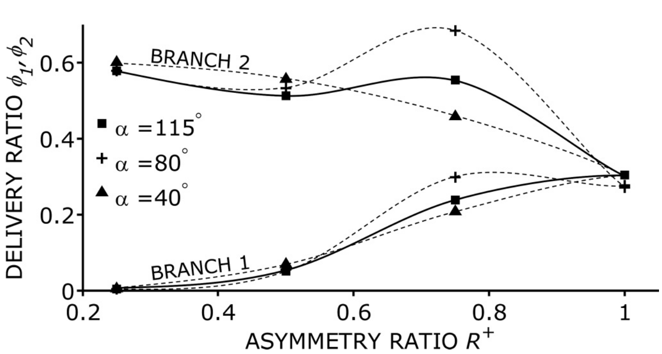

FIG. 12. Delivery ratios through the daughter branches as functions of the asymmetry ratio.

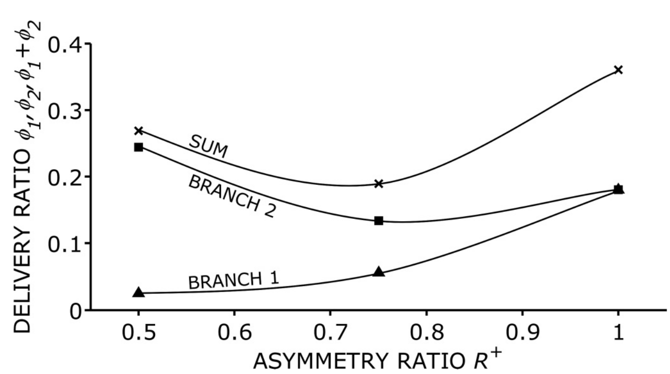

FIG. 14. Delivery ratios through the daughter branches and their sum without widening of the parent branch. The branching angle is constant at $\alpha = 115^\circ$.

larger than 90° (see Fig. 9). This behavior is caused by the saturated wall displacement in combination with the increasing flux resistance. In summary, the optimal branching angle is a consequence of two counteracting mechanisms: pressure rise due to wall elasticity, particularly at the bifurcation entrance, and viscous fluid friction due to flow momentum redirection.

In Fig. 11 it can be seen that for rigid vessel walls the optimal mass flux occurs for small branching angles. Thus the bifurcation represents simply a fluidic resistance which increases with increasing branching angle. Without the additional structural response of the elastic vessel wall the optimal branching angle of about $\alpha = 90°$ does not exist.

B. Asymmetry ratio

Due to the changes in diameter (see Fig. 3) the mass flux through branch 1 increases, while the mass flux through branch 2 decreases with increasing asymmetry ratio. An optimal asymmetry ratio of about 0.75 is found for a wide range of branching angles (see Fig. 7). The vessel wall displacement ΔL is also maximal for $R^+ \approx 0.75$ (see Fig. 13). The reason for the asymmetry dependent displacement can be found by analyzing the data presented in Fig. 6. From left to right the velocity and shear field for asymmetry ratios R^+ of 0.5, 0.75, and 1.0 are compared for branching angles of 80° and 115°. A low asymmetry ratio means that the diameter of daughter branch 2 and the diameter of the parent branch are similar. Thus, in the present study, a small asymmetry ratio represents basically a curved vessel without stagnation point. The velocity field shows that the flow pattern smoothly resembles the curvature of branch 2 for $R^+ = 0.5$. Increasing R^+ to 0.75 shifts the position of the branching tip towards the center of the geometry and causes the formation of a stagnation point for the fluid flow. Figure 14 shows the mass flux in a rigid geometry. It indicates that the lowest mass flux occurs for $R^+ \approx 0.75$. This is apparently the asymmetry ratio with the highest flow resistance.

Returning to the case of an elastic vessel, the flow stagnation increases the pressure at the bifurcation entrance and, thus, the wall displacement ΔL. As a consequence, an increase in maximal mass flux occurs during the tightening phase of the vessel. Increasing R^+ further towards 1.0 yields a decrease in wall displacement as well as a decrease of the combined daughter branch mass flux (see Figs. 13 and 8). Taking Eq. (1) into account, the total outlet area of the bifurcation, $\pi(R_1^2 + R_2^2)$, increases with increasing asymmetry ratio. The reduced flow stagnation associated with the larger outlet area appears to reduce the pressure and, thus, the wall displacement at the bifurcation entrance for $R^+ > 0.75$. In summary, the competing mechanisms of rising pressure due to enhanced flow stagnation and falling pressure due to enlarged outflow area yield a distinct optimum of the asymmetry ratio R^+. Again, the vessel wall elasticity is a key requirement for the observed geometry optimum.

C. Comparison with experimental findings

The physiological validity of the computational fluid dynamic approach is not clear yet. Therefore, the results are compared with the findings from Cassot *et al.* who created a database of bifurcation patterns in the human cerebral cortex based on the analysis of 10 000 samples [18]. Table I summarizes the obtained statistics of the branching angles. It also gives information about the population of the vessel type and the group of vessels. Cassot *et al.* also analyzed the area asymmetry ratio A_1/A_2 of the daughter branches. This can be compared to R^+ after taking the square root. They observed a mean area asymmetry ratio $A_1/A_2 = 0.686$ and, thus, $\sqrt{A_1/A_2} = 0.828$. In Fig. 15 the mean values and standard deviations for α found for parent vessel orders 1 and 4, respectively, as well as the mean value of $\sqrt{A_1/A_2}$ are displayed in comparison to the WSS results from the present study. Only angles for vessel order 1 and 4 are shown because order 2 and 3 are in between. The majority of the experimentally observed geometries are located within the parameter space yielding a WSS >1.5 Pa. The WSS of 1.5 Pa is known for its stimulation of gene expressions which protects against arteriosclerosis and platelets activation. Even if taking the geometries within the standard deviations of parent vessel order 1 and 4 into account, the data points are still within the region of a WSS >1 Pa, which is known to be the minimum for healthy conditions without increased risk of thrombus formation. Thus the experimentally studied, natural bifurcations confirm the numerically found bifurcation geometries which are optimized with respect to the WSS stimulation. The experimentally observed mean asymmetry ratio of 0.828 differs by 7.7% from the numerical optimum of $R^+ = 0.769$ and the observed mean branching angle of 102.84° differs by 13.3% from the numerical optimum of $\alpha = 90.7°$.

The spread is within the standard derivation of branching angles of each parent vessel order. Thus a given branching

TABLE I. Experimental findings for branching angle α taken from Cassot *et al.* [18].

	Vessel nature		Parent vessel topological order			
Group	Arterioles	Venules	1	2	3	4
Crebrity	57.7%	42.3%	71.3%	21.7%	6.66%	0.34%
Mean α	108°	99°	107°	97°	88°	82°
Standard deviation	28°	24°	26°	28°	29°	24°

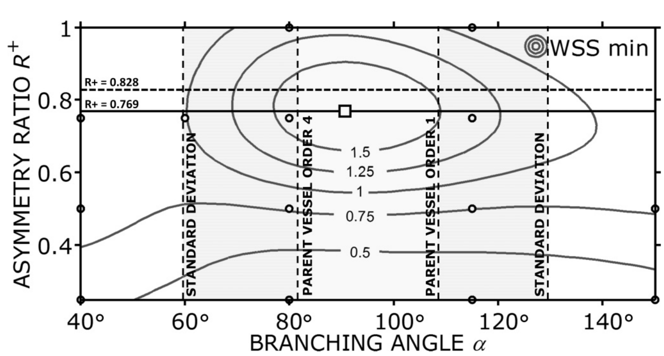

FIG. 15. Comparison of simulation results and experimentally obtained bifurcation geometries.

angle cannot be assigned to a unique vessel order within the group of arterioles. This geometrical similarity within the group of arteriole vessels is utilized to understand the role of wall elasticity and WSS on the physiological bifurcation pattern by using a simplified arterioles model with a low number of geometrical properties.

D. Model applicability and limitations

The present work assumes an exponent of 3 in Murray's law, Eq. (1). However, Cassot *et al.* found a range of exponents for Murray's law for different parent vessel topological orders, which are 3.98, 2.73, 2.75, and 2.89 for the vessel orders 1 to 4, respectively. Therefore, the current simulation model geometries are especially comparable to the vessel orders 2, 3, and 4. The mean branching angle of these vessel orders is 93.5°. It differs from the numerically computed optimum only by 3.1%. This circumstance suggests that the simulation model geometries are appropriate for a range of arteriole vessel types. However, the applicability of the simulation model might be extended if the exponent in Murray's law is chosen not to be fixed at a value of 3.

A key factor for the bifurcation geometry is the wall elasticity. The assumption of rigid walls would lead to an optimal geometry with low branching angles and equal radii of the daughter branches. The question arises whether the found geometry patterns are also applicable to other vessel types such as arteries and capillaries with different wall elasticity. Due to the muscles within the vessel walls, arteries are stiffer than arterioles. Yet, the flux is higher as well and, thus, it also widens the vessel. It is therefore likely that the bifurcation geometries of arterioles and arteries share design features, but they do not necessarily have the same branching angles and asymmetry ratios. In the case of capillaries, the wall stiffness is relatively high compared to the flux. The blood pressure on the wall may not lead to a significant vessel widening. Thus, in capillaries, it is not expected that the elasticity contributes to the geometry of the bifurcations. This should lead to low branching angles and rather symmetric bifurcations. An experimental study would be required to verify this hypothesis.

The present study shows that details of the bifurcation geometry of arterioles are obtained by optimizing the mechanical stimulation of the endothelial cells at the vessel walls due to the WSS. However, for the description of a complete vascular tree the distribution of vessel diameters and the positions of bifurcations are required. These quantities cannot be obtained by a WSS optimization. They require an optimization of the energy balance of the system. Thus the present observations on the length scale of individual bifurcations do not contradict the idea of optimizing the energy cost function of the vascular tree but rather complement it. In other words, different optimization principles seem to exist on different length scales.

V. CONCLUSION

Computational fluid structure interaction simulations with physiological boundary conditions were performed in order to study vascular bifurcations. The physiologically significant WSS in a bifurcation was analyzed and the homogeneity of the WSS was the subject of a geometrical optimization procedure. The geometrical details of a bifurcation were represented by two dimensionless parameters, namely the radius asymmetry ratio of the daughter branches and the branching angle between them. A design of experiments approach was used in order to keep the numerical effort as small as possible while preserving its predictive power.

With this simulation model we were able to describe the fluid dynamics and solid mechanics processes which influence the geometry of an optimal bifurcation. A range of branching angles and asymmetry ratios yielding physiological WSS conditions were identified. The optimal geometry could be validated by comparison with the experimental data of 10 000 natural bifurcations.

A. Impact on clinical diagnostics

Bifurcations are known as the initial point for vascular diseases, such as thrombus formation and atherosclerosis, due to pathological flow conditions. However, the detection of growing occlusions by measuring the modified blood flux requires an advanced stage of the disease. Hence state of the art clinical diagnoses could be improved by an earlier identification of atherosclerosis. With the findings of the present study the question arises whether the detection of pathological bifurcation geometries may lead to an earlier diagnosis of vascular diseases. Instead of analyzing the blood flow to identify occlusions, it might be reasonable to analyze branching geometries in the first place since those change prior to the mass flux. Pathological regions could be detected before occlusions or even reductions in the blood flow are measurable.

B. Impact on tissue engineering

Artificial vascularization is one of the key challenges in tissue engineering. It is possible to build artificial vascular structures based on the derived optimal bifurcation geometries using additive manufacturing techniques. The local bifurcation design can be coupled with existing design approaches for the network structure of vascular systems. In tissue engineering, such vascular networks can then be used to supply cells in large volumes for extended time spans. The cultivation of complex cell structures and organs becomes imaginable since nowadays the missing vascularization is a major bottleneck for those developments.

VI. OUTLOOK

The present study addresses the shear stress distribution in bifurcations and focuses on its inhomogeneity. A single phase fluid model is utilized to simulate the perfusion of different branching geometries. This model yields a geometrical optimum with respect to physiological flow conditions aiming at the avoidance of plaque formation. Even though the WSS has been identified as a major parameter for atherosclerosis, the actual mechanisms on the scale of the suspended particles are not yet fully understood. Hemostasis plays an important role in atherosclerotic initiation [36,37]. Mechanisms such as platelet adhesion occur dependent on the experienced shear stress. Thus a multiphase fluid approach could treat the question in which way platelet adhesion promotes atherosclerotic initiation.

ACKNOWLEDGMENTS

This work was supported by the FhG Internal Programs under Grant No. MAVO BioRap. The research leading to these results has received funding from the European Union Seventh Framework Programme (FP7/2007-2013) under Grant No. 263416.

[1] C. G. Caro, Arterioscler. Thromb. Vasc. Biol. **29**, 158 (2009).
[2] A. Malek, S. L. Alper, and S. Izumo, JAMA, J. Am. Med. Assoc. **282**, 2035 (1999).
[3] R. G. Mason, D. Sharp, H. Y. Chuang, and S. F. Mohammad, Arch. Path. Lab. Med. **101**, 61 (1977).
[4] D. Shweiki, A. Itin, D. Soffer, and E. Keshet, Nature **359**, 843 (1992).
[5] A. Zakrzewicz, T. W. Secomb, and A. R. Pries, Physiology **17**, 197 (2002).
[6] P. F. Davies, Physiol. Rev. **75**, 519 (1995).
[7] M. Bongrazio, Ph.D. thesis, Freie Universität Berlin, 2004.
[8] J. C. de Graaf, J. C. Banga, S. Moncada, R. M. J. Palmer, P. G. de Groot, and J. J. Sixma, Circulation **85**, 2284 (1992).
[9] C. Murray, Proc. Natl. Acad. Sci. USA **12**, 207 (1926).
[10] C. Murray, Proc. Natl. Acad. Sci. USA **12**, 299 (1926).
[11] G. S. Kassab and Y. C. Fung, Ann. Biomed. Eng. **23**, 13 (1995).
[12] A. Kamiya and T. Togawa, Bull. Math. Biophys. **34**, 431 (1972).
[13] M. Kretowski, Y. Rolland, J. Bézy-Wendling, and J. L. Coatrieux, Comput. Meth. Prog. Biomed. **70**, 129 (2003).
[14] W. Schreiner, R. Karch, M. Neumann, F. Neumann, P. Szawlowski, and S. Roedler, Med. Eng. Phys. **28**, 416 (2006).
[15] G. Hamarneh and P. Jassi, Comput. Med. Imag. Graph. **34**, 605 (2010).
[16] G. S. Kassab, C. A. Rider, N. J. Tang, and Y. C. Fung, Am. J. Physiol. **265**, H350 (1993).
[17] G. S. Kassab, D. H. Lin, and Y. C. Fung, Am. J. Physiol. **267**, H2100 (1994).
[18] F. Cassot, F. Lauwers, S. Lorthois, P. Puwanarajah, V. Cances-Lauwers, and H. Duvernoy, Brain Res. **1313**, 62 (2010).
[19] E. C. Novosel, C. Kleinhans, and P. J. Kluger, Adv. Drug Deliv. Rev. **63**, 300 (2011).
[20] J. S. Miller, K. R. Stevens, M. T. Yang, B. M. Baker, D. H. T. Nguyen, D. M. Cohen, E. Toro, A. A. Chen, P. A. Galie, X. Yu, R. Chaturvedi, S. N. Bhatia, and C. S. Chen, Nat. Mater. **11**, 768 (2012).
[21] Y. Zheng, J. Chend, M. Cravenc, N. W. Choic, S. Totoricae, P. K. A. Diaz-Santanac, B. Hempsteadf, C. Fischbach-Teschlg, J. A. Lópezd, and A. D. Stroockc, Proc. Natl. Acad. Sci. USA **109**, 9342 (2012).
[22] G. West, J. H. Brown, and B. J. Enquist, Science **276**, 122 (1997).
[23] G. Hutchins, M. M. Miner, and J. K. Boitnott, Circ. Res. **38**, 572 (1976).
[24] M. Zamir and J. Medeiros, J. Gen. Physiol. **79**, 353 (1982).
[25] H. N. Mayrovitz and J. Roy, Am. J. Physiol. **245**, H1031 (1983).
[26] C. Hirt, Proc. Second Intl. Conf. Numer. Meth. Fluid Dyn. **8**, 350 (1971).
[27] S. Chien, S. Usami, R. J. Dellenback, and M. I. Gregersen, Science **157**, 829 (1967).
[28] S. Chien, S. Usami, R. J. Dellenback, and M. I. Gregersen, Science **157**, 827 (1967).
[29] K. Yasuda, Ph.D. thesis, Massachusetts Institute of Technology, 1979.
[30] S. Chien, Red Blood Cell **2**, 1031 (1975).
[31] L. Formaggia, J. F. Gerbeau, F. Nobile, and A. Quarteroni, SIAM J. Numer. Anal. **40**, 376 (2003).
[32] R. F. Schmidt, F. Lang, and M. Heckmann, *Physiologie des Menschen* (Springer, Berlin, 2010).
[33] P. Raback, M. Malinen, J. Ruokolainen, A. Pursula, and T. Zwinger, *Elmer Models Manual* (CSC–IT Center for Science Ltd., Espoo, Finnland, 2016).
[34] D. Ku, D. Giddens, C. Zarins, and S. Glagov, Arterioscler. Thromb. Vasc. Biol. **5**, 293 (1985).
[35] D. G. Krige, J. Chem. Metall. Min. Soc. S. Africa **52**, 119 (1951).
[36] S. Massberg, K. Brand, S. Grüner, S. Page, E. Müller, I. Müller, W. Bergmeier, T. Richter, M. Lorenz, I. Konrad, B. Nieswandt, and M. Gawaz, J. Exp. Med. **196**, 887 (2002).
[37] J. Borissoff, H. M. H. Spronk, and H. ten Cate, New England J. Med. **364**, 1746 (2011).